ELSEVIER

Colloids and Surfaces
A: Physicochemical and Engineering Aspects 175 (2000) 179–192

COLLOIDS AND SURFACES A

www.elsevier.nl/locate/colsurfa

Effect of surfactants on the stability of films between two colliding small bubbles

Dimitrina S. Valkovska, Krassimir D. Danov *, Ivan B. Ivanov

Laboratory of Thermodynamics and Physico-Chemical Hydrodynamics, Faculty of Chemistry, University of Sofia, James Bourchier Ave. 1, 1164 Sofia, Bulgaria

Abstract

The stability of partially mobile drainage thin liquid film formed between two slightly deformed approaching bubbles or drops is studied. The intervening film is assumed to be thermodynamically unstable. The material properties of the interfaces (surface viscosity, Gibbs elasticity, surface and bulk diffusion) are taken into account. To examine the stability of the thin film we consider the coupling between the drainage and the disturbance flows. The velocity and pressure distributions due to the drainage flow are obtained by using the lubrication approximation. The disturbance flow is examined by imposing small perturbations on the film interfaces and liquid flow. The long wave approximation is applied. We solved the linear problem for the evolution of the fluctuations in the local film thickness, interfacial velocity and pressure. The linear stability analysis of the gap region allows us to calculate the critical thickness, at which the system becomes unstable. Quantitative explanation of the following effects is proposed, (i) the increase of critical thickness with the increase of the interfacial mobility; (ii) the role of surface viscosity, compared with that of the Gibbs elasticity; (iii) the significant destabilization of the gap region with the decreasing droplet radius in the case of buoyancy driven motion. The analytical expressions for critical thickness in the case of negligible surface viscosity and tangentially immobile interfaces are presented.

Keywords: Small bubbles or drops; Thin liquid film stability; Critical thickness; Influence of surfactants; Interfacial mobility

1. Introduction

The stability of thin films is an important problem in understanding the stability of foams and emulsions. Due to the great industrial and scientific interest many authors have studied the stability problem, both experimentally and theoretically. In foam systems the bubbles are large enough and when they approach each other at a given distance they may change their shapes. The plane-parallel films are formed, which keep their radii almost constant during the process of thinning. On the contrary, in most of the emulsion systems the drops are very small (the radii are of the order of several microns) and due to the high capillary pressure they approach one to the other without significant change of their spherical shapes. In both the cases due to the thermal or

* Corresponding author. Tel.: +359-2-9625310; fax: +359-2-9625643.

E-mail address: krassimir.danov@ltph.bol.bg (K.D. Danov).

0927-7757/00/$ - see front matter
PII: S0927-7757(00)00621-X

mechanical fluctuations, which lead to the corrugations of the film surfaces, the films rupture or black spot may form. The corrugations at the film interfaces give rise to two forces: the first one, caused by capillary pressure, tends to resist any deformation of the surfaces, while the second one, due to the increase in negative disjoining pressure, tends to increase the amplitude of the corrugations.

Because of the existence of a lot of experimental methods for investigation of almost plane-parallel films (Scheludko cell, etc.), there are many theoretical and experimental studies which examine their stability. Numerous experiments have shown [1,2] that even when the liquid films are plane-parallel, they never thin to zero thickness but rupture, or black (thinner) spots form at a finite thickness of the order of 50 nm, called critical thickness [2]. De Vries [3,4] pointed out that the local fluctuations of the film thickness (which are always present because of either mechanical perturbations or thermal fluctuations) led to two opposite effects. The first one is the positive contribution to the free energy due to the increase of the film area and the second one is the negative contribution resulting from the increased negative van der Waals energy of interaction in the thinner parts. Vrij [5] and Vrij and Overbeek [6] predicted the critical thickness for non-thinning films of infinite extend. Their results show that the critical thickness is independent of the viscosity of the film and is proportional to 2/7 power of the film radius. Lucassen et al. [7] extended Vrij's analysis to illustrate the effects of interfacial tension, interfacial elasticity, adjoining phases and gravity. Ivanov et al. [8] analyzed the stability of thinning films containing high and low surfactant concentration. Later Ivanov and Dimitrov [9] included the effects of surface diffusion and surface viscosity and showed that the decrease in critical thickness with increasing surfactant concentration is due to surface viscosity. Malhotra and Wasan [10] examined the stability of radial bounded film with tangentially immobile interfaces and indicated the significant effect of the drainage flow. The alternative approach was studied by Chen and Slattery [11] and Yiantsios and Davis [12]. These authors studied numerically the deformation of two approaching small droplets in pure liquid phases (no surfactant present) under the action of an external driving force and van der Waals attraction force. They found two different regimes: without dimple formation and with dimple formation. They also showed that at a given gap width, h_{pt}, the van der Waals attraction can prevail over the hydrodynamic resistance and observed at even small thickness increase of the curvature in the gap region (a pimple appears). Therefore, Chen and Slattery [11] and Yiantsios and Davis [12] consider the rupture to be a natural evolution of the drop shapes rather than instability.

The problem for stability of the gap between two slightly deformed drops has been weekly studied up to now. The main reason is the great difficulty in preparing and performing the experimental investigations because of the small drop radii. Recent years Lean-Calderon et al. [13] and Mondain-Monval et al. [14] reported a direct measurement of the short distance profiles between small emulsion droplets in surfactant solution of various aspects.

This study investigates the stability of the gap between two slightly deformed bubbles (drops), which approach each other under the action of an external force. The intervening film is assumed to be thermodynamically unstable. The lubrication approximation is used to describe the drainage and disturbance flows. The material properties of the interfaces are taken into account (see the tangential and normal stress boundary conditions in Section 2). The linear stability analysis of the gap region is applied. The analytical expressions for critical thickness (Section 3) provide information about the influence of surfactants on the bubbles stability. Numerical results, based on nonionic and ionic surfactants and protein isolates, show a significant dependence of the critical thickness on the mobility of the interfaces (see Section 4).

2. Mathematical model of the problem

We consider a thin viscous liquid layer, formed between two bubbles, which flows out due to their approach under the action of the external force, F

(see Fig. 1(a)). For the sake of simplicity we assume that the two bubbles have the same radii, R_c. The problem is described in a cylindrical coordinate system, Orz, and the local thickness of the layer is denoted by $H(r, t)$. Since the bubbles are close to each other, the hydrodynamic resistance is concentrated in the gap region. In the gap region the radii of the curvature are larger compared with the local film thickness, therefore, the lubrication approximation can be applied (see the main requirement for this approximation (i), (iii) and (iv) [15]).

2.1. Basic equations in lubrication approximation

In lubrication approximation the pressure, P, in the continuos phase depends only on the radial coordinate, r, and time, t, $P = P(r, t)$. After integration of the equations of fluid motion and continuity, with account for the corresponding kinetimatic boundary conditions, the integrated bulk continuity equation is obtained:

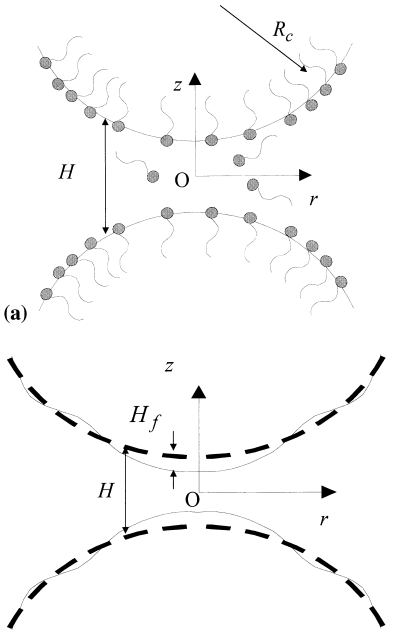

Fig. 1. Sketch of two approaching bubbles of radii R_c separated at a distance H, (a) basic state; (b) small fluctuations on the surfaces.

$$\frac{\partial H}{\partial t} + \frac{1}{r}\frac{\partial}{\partial r}\left[rH\left(U - \frac{H^2}{12\eta}\frac{\partial P}{\partial r}\right)\right] = 0 \quad (1)$$

In Eq. (1) η is the dynamic viscosity and U is the radial component of the surface velocity.

We assume that the surfactant, present in the film, is soluble only in the continuos phase. Then in the case of emulsion systems (two approaching drops), the viscous friction due to the disperse phase is negligible compared with the viscous friction due to the continuos phase. Therefore, the emulsion system behaves as foam — so called 'foam film approach' (see Eqs. (25a) and (25b) and the discussion below [16]). Hence our results are applicable for both foam and emulsion systems.

The surfactant distribution can be calculated by solving the diffusion equation along with the surfactant balance at the film surfaces and the assumption for small Peclet number in the gap region. We also assume small deviation from equilibrium of the subsurface concentration and adsorption that the surface material parameters remain constant during the drainage. In the literature this is a usual simplification for solving the drainage and stability problems. Usually in thin liquid films the surfactant exchange between the bulk fluid and the interfaces is diffusion-controlled [16,17].

The boundary condition for the balance of surface excess linear momentum takes into account the influence of the surface viscosity (Boussinesq effect) and the surface tension gradient (Marangoni effect). Using the above assumptions the dependence of the adsorption, Γ, on the surface velocity, U, and the local film thickness, H, can be obtained from the solution of the diffusion problem. Then the Marangoni term in the tangential stress balance boundary condition has an explicit form and the tangential stress balance boundary condition simplifies to [15,17]

$$\frac{H}{12\eta R_c}\frac{\partial P}{\partial r} = -\frac{U}{R_c(h_s + bH)} + N_{sv}\frac{\partial}{\partial r}\left[\frac{1}{r}\frac{\partial}{\partial r}(rU)\right] \quad (2)$$

The parameters, b, h_s, and N_{sv}, in Eq. (2) take into account the effects of the bulk and surface diffusions and the surface viscosity. They are defined by the relationships

$$b \equiv \frac{3\eta D}{h_a E_G}, \qquad h_s \equiv \frac{6\eta D_s}{E_G}, \qquad N_{sv} \equiv \frac{\eta_s}{6\eta R_c} \tag{3}$$

In Eq. (3) $E_G \equiv -\partial\sigma/\partial \ln \Gamma$ is the equilibrium value of the Gibbs elasticity and $h_a \equiv \partial\Gamma/\partial c$ is the equilibrium value of the adsorption length, which characterizes the slope of the adsorption isotherm. The surface tension is σ, the bulk and surface diffusion coefficients are D and D_s, and the sum of the interfacial shear, η_{sh}; and dilatational, η_{dil}; viscosities is the total surface viscosity, $\eta_s \equiv \eta_{sh} + \eta_{dil}$. The parameters defined by Eq. (3) do not depend on the film thickness. They can vary in a wide range depending only on the type of surfactants and the surfactant concentration (see Section 4).

In lubrication approximation the normal stress boundary condition reduces to balance of pressures:

$$P_m + \frac{2\sigma}{R_c} = P + \Pi + \frac{\sigma}{2r}\frac{\partial}{\partial r}\left(r\frac{\partial H}{\partial r}\right) \tag{4}$$

where, P_m is the pressure in the meniscus at infinity, and Π is the disjoining pressure.

Finally, the force balance equation, which in quasi-steady state approach expresses the balance between the external force and hydrodynamic drag and intermolecular forces, reduces to

$$F = 2\pi \int_0^\infty (P + \Pi - P_m) r dr \tag{5}$$

Eqs. (1)–(5) entirely describe the drainage flow, the shape of the bubbles and the long wave stability of the gap between the bubbles.

2.2. Drainage flow

In the case of small bubbles the thickness at which the instability due to the fluctuations appears is higher than the thickness of plane-parallel film formation. Therefore, the drainage flow is described by the leading order solution of the problem, when the drops still have spherical form [15,18]. In lubrication approximation the spherical shape of the bubbles is approximated by parabola, H_{up}. Hence, the leading order of the film thickness is

$$H_{up}(r, t) = h(t) + \frac{r^2}{R_c} \tag{6}$$

where, $h(t)$ is the minimal distance between the bubbles (see Fig. 1(a)).

As it was shown [15], because of the boundary conditions at $r = 0$ and infinity, it is convenient to present the leading order solution for the unperturbed surface velocity, U_{up}, as a Fourier series:

$$U_{up} = \frac{V}{2}\sqrt{\frac{R_c}{h}} \sum_{k=1}^{\infty} a_k \sin(k\theta) \tag{7}$$

In Eq. (7) the constants a_k ($k = 1, 2, \ldots$) depend implicitly on the physical parameters and the distance between the bubbles, h. The leading order of the approaching velocity is $V \equiv -\mathrm{d}h/\mathrm{d}t$ and the new variable, θ, is defined as $\tan(\theta/2) \equiv r/\sqrt{hR_c}$. Then the relationship for the approaching velocity takes the form:

$$V = \frac{2h}{3\pi\eta R_c^2}\left(F - 2\pi \int_0^\infty \Pi r dr\right)\Phi_v,$$

$$\Phi_v = \frac{1}{1 - a_{odd} + a_{ev}} \tag{8}$$

The mobility function, Φ_v, takes into account the influence of the rheological parameters and is calculated for several asymptotic cases [18]. Φ_v is a complex function of the thickness, h, and the material properties of the interfaces through the parameters b, h_s, and N_{SV}. In Eq. (8) a_{odd} and a_{ev} are the respective sums of the odd and even parts of the coefficients a_k:

$$a_{odd} = \sum_{k=0}^{\infty} \frac{a_{2k+1}}{2(2k+1)}, \qquad a_{ev} = \sum_{k=1}^{\infty} \frac{k a_{2k}}{4k^2 - 1} \tag{9}$$

The above equations (Eqs. (6)–(9)) completely define the leading order of the basic state of approach of two spherical bubbles. The next order approximation for the shape with respect to the capillary number function has been calculated [18]. Therein the expressions for the inversion thickness, at which the film appear, and for the pimple thickness, at which due to the attractive van der Waals force the gap thickness spontaneously decreases, have been derived. It is important to note that when the disjoining pressure has a large positive value (repulsion between the drop interfaces) the velocity of approach, V, in Eq. (8) can be 0. Therefore, at this gap width the approach of drops stops and the film between them

is thermodynamically stable. It is the case of a strong electrostatic repulsion due to an ionic surfactant adsorption or of a strong steric interaction between the interfaces when the film is stabilized with protein isolates. We will consider only the thermodynamically unstable films. In such a case the time scale of the fluctuations arising from the thermal or mechanical corrugations of the interfaces can be rather different than the time scales for the inversion and pimple thickness. For that reason the fluctuation analysis of the problem is developed below.

2.3. Linear stability analysis

Due to thermal fluctuations or other disturbances at a given thickness the film surfaces start to corrugate (Fig. 1(b)). For the linear stability analysis of the system (Eqs. (1)–(5)) we introduce small perturbations of the pressure, P_f; interfacial velocity, U_f; and shape, H_f; with respect to the leading order of the drainage flow. We assume that H_f is much smaller than the wavelength, i.e. we apply the long wave limit. We replace the physical parameters of the system, P, U, and H, by $P_{up}+P_f$, $U_{up}+U_f$, and $H_{up}+H_f$. The resulting system of equations is linearized with respect to the perturbations. Then the final form of the continuity equation (Eq. (1)) for the fluctuation reads

$$\frac{\partial H_f}{\partial t}+\frac{1}{r}\frac{\partial}{\partial r}\left[r\left(U_{up}-\frac{H_{up}^2}{4\eta}\frac{\partial P_{up}}{\partial r}\right)H_f\right]+\frac{1}{r}\frac{\partial}{\partial r}\left[rH_{up}\left(U_f-\frac{H_{up}^2}{12\eta}\frac{\partial P_f}{\partial r}\right)\right]=0 \tag{10}$$

From the tangential stress boundary condition (Eq. (2)) for the linear term in the perturbed quantities one obtains:

$$\frac{H_{up}}{12\eta R_c}\frac{\partial P_f}{\partial r}=-\frac{U_f}{R_c(h_s+bH_{up})}+N_{sv}\frac{\partial}{\partial r}\left[\frac{1}{r}\frac{\partial}{\partial r}(rU_f)\right]+\left[\frac{bU_{up}}{R_c(h_s+bH_{up})^2}-\frac{1}{12\eta R_c}\frac{\partial P_{up}}{\partial r}\right]H_f \tag{11}$$

Similarly, the normal stress boundary condition (Eq. (4)) gives the form:

$$P_f+\Pi'(H_{up})H_f+\frac{\sigma}{2r}\frac{\partial}{\partial r}\left[r\frac{\partial H_f}{\partial r}\right]=0 \tag{12}$$

The derivatives of the disjoining pressure depend on the unperturbed local thickness, H_{up}, and they are the functions of radial coordinate, r, and time, t: $\Pi^{(n)}(H_{up})\equiv\partial^n\Pi/\partial H_{up}^n$ ($n=1, 2, \ldots$); it follows that the fluctuation in the film profile must disappear at infinity: $\partial H_f/\partial \ln r\to 0$ at $r\to\infty$.

From mathematical viewpoint the linear stability problem (Eqs. (10)–(12)) is a system of differential equations with coefficients depending on the radial coordinate, r, and time, t. For the solution of such problems the fluctuation parameters can be represented as the superposition of Fourier–Hankel components with different wave numbers and amplitudes. Then the fluctuation in the surface shape can be presented by the following integral transformation:

$$H_f=\int_0^\infty \tilde{H}_f(t,k)J_0(kr)k\,dk \tag{13}$$

where, $\tilde{H}_f(t,k)$ is the image of the film profile fluctuation, k is the radial wave number, and J_0 is the zero order Bessel function.

According to the DLVO theory, if the slope of the disjoining pressure isotherm is positive, $\partial\Pi/\partial H_{up}>0$, the system is unstable and the amplitude of the corrugations in the zone of contact increases. For every Fourier–Hankel component there is a film thickness at which the respective surface fluctuation becomes unstable and this surface corrugation begins to grow spontaneously. The maximum of these thicknesses (called the *transitional thickness* [9,16]) corresponds to the moment at which the instability appears for the first time. Short time after the transitional thickness is reached the film reaches the critical thickness and breaks. For gap distances larger than the transitional thickness all fluctuations are stable. We will assume that there are no forces, which are strong enough to hold the two surfaces apart; consequently, the film breaks and the bubbles coalesce. It is shown below (see Section 4) that most often the hydrodynamic resistance in the

case of slightly deformed bubbles is much lower than that in the case of plane-parallel film, and the fluctuations grow very fast after the transitional thickness. For that reason we will disregard the difference between the transitional and the critical thickness and will call all parameters pertaining to the transitional thickness 'critical'.

3. Calculation of the critical thickness

3.1. General case

The main difficulty with the solution of the system (Eqs. (10)–(13)) is the different types of equations. In fact, the fluctuation in the dynamic pressure, P_f, can be easily found from the integral representation (Eq. (13)) and the normal stress boundary condition (Eq. (12)) to be

$$P_f = \int_0^\infty \left(\frac{\sigma k^2}{2} - \Pi'\right)\tilde{H}_f\, J_0(kr)kdk \tag{14}$$

But the order of Eqs. (10) and (11) for the fluctuation in the surface velocity, U_f, is different. In order to eliminate U_f the integrated bulk continuity equation (Eq. (10)) and the tangential stress boundary condition (Eq. (11)) are rewritten in the equivalent forms:

$$\frac{\partial U_f}{\partial r} + \left(\frac{1}{r} + \frac{2r}{R_c H_{up}}\right)U_f + L[H_f, P_f] = 0 \tag{15}$$

$$N_{sv}\frac{\partial^2 U_f}{\partial r^2} + N_{sv}\frac{1}{r}\frac{\partial U_f}{\partial r} - \left[\frac{N_{sv}}{r^2} + \frac{1}{R_c(h_s + bH_{up})}\right]U_f + M[H_f, P_f] = 0 \tag{16}$$

where, L and M are linear differential operators depending on the fluctuations H_f and P_f. The definitions of L and M are given by Eqs. (A.1) and (A.2) in Appendix A. Then, from Eqs. (15) and (16) the function U_f is calculated (see Eq. (A.4) in Appendix A). After substitution of Eq. (A.4) into Eq. (15) the following operator equation is derived:

$$L - \frac{1}{rH_{up}}\frac{\partial}{\partial r}\left\{\frac{R_c^2 H_{up}^2 r(h_s + bH_{up})}{R_c H_{up}^2 - 8N_{sv}r^2(h_s + bH_{up})}\left[N_{sv}\left(\frac{\partial L}{\partial r} - \frac{2r}{R_c H_{up}}L\right) - M\right]\right\} = 0 \tag{17}$$

Eq. (17) contains only the fluctuations in the film profile, H_f, and the dynamic pressure, P_f. If we replace the fluctuations H_f and P_f with their integral forms Eqs. (13) and (14) the final form of the dispersion equation for the image, $\tilde{H}_f$, is obtained. The dispersion relation is a complex function of the time and the radial coordinate and it is impossible to derive the original Fourier–Hankel image. Nevertheless the most probable region for the film rupture is the gap between the interfaces. For that purpose we investigate the stability of the system at small radial distances, i.e. the limit $r \to 0$.

The basic state (without any perturbations) depends on time (the gap thickness, h, decreases), that is why the ratio between the perturbed and unperturbed states is the relevant characteristic of the stability. In fact, $\tilde{H}_f$ can decrease with the decreasing of h, but the ratio $\tilde{H}_f/h$ can still increase. Therefore, we represent the perturbation in the form $\tilde{H}_f = h\bar{H}_f$. If the amplitude $\bar{H}_f$ decreases with time the film is stable, and if it increases the respective fluctuations are unstable.

After the asymptotic limit of Eq. (17) for $r \to 0$, the stability problem for the amplitude, $\bar{H}_f$, reduces to

$$-\frac{q_0(h) + q_2(h)k^2}{\bar{H}_f}\frac{\partial \bar{H}_f}{\partial t} = Y(h, k) \tag{18}$$

where, $Y(h, k) \equiv g_0(h) + g_2(h)k^2 + g_4(h)k^4 + g_6(h)k^6$. The final forms of the coefficients appearing in Eq. (18) are given in Appendix B. The functions q_0, q_2, g_0, g_2, g_4, g_6 depend on $h(t)$ and also on the parameters b, h_s and N_{SV}, which take into account the influence of the surfactant. When the derivative $\partial\bar{H}_f/\partial t$ is positive the fluctuations of the shape spontaneously grow. In the opposite case ($\partial\bar{H}_f/\partial t < 0$) the amplitudes of the fluctuations decrease with time. The stability limit is defined as the gap thickness at which the first solution of the equation $\partial\bar{H}_f/\partial t < 0$ appears. The typical behavior of the function Y for different film thickness versus wave number is illustrated in Fig. 2. In the case of van der Waals attractive forces (see Fig. 2) for all gap distances, h, the function Y is minimum. The instability takes place when $Y(k, h) = 0$. If for given gap distance the function Y is positive for all wave numbers, k,

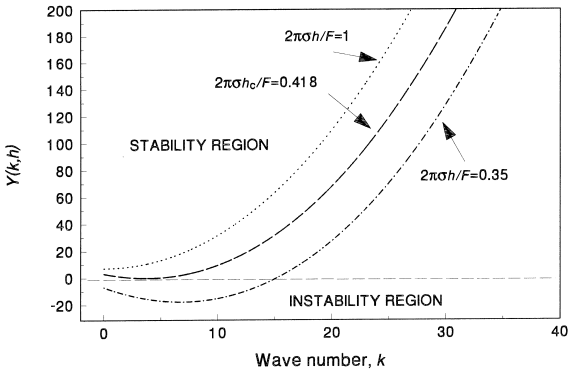

Fig. 2. Typical behavior of the function, $Y(h, k)$, vs. wave number, k, for different values of the nondimensional film thickness, $2\pi\sigma h/F = 1$; $2\pi\sigma h_c/F = 0.418$; and $2\pi\sigma h/F = 0.35$.

then at this thickness the film is stable for any k. On the contrary, if the function Y, at a given thickness, has negative value then the corresponding fluctuation grows with time. Therefore, the transitional (critical) thickness is the maximal thickness at which the instability first appears (see Fig. 2). The corresponding wave number at this point is the critical wave number, k_c. In the general case the critical wave number, k_c, and the corresponding critical thickness, h_c, can be found only numerically. The results from the computations are given in Section 4. In the case of tangential immobile interfaces or negligible surface viscosity the asymptotic expressions for the critical thickness are derived in Section 3.2 below.

3.2. Negligible surface viscosity

In the case of low molecular weight surfactants at small surfactant concentration the effect of surface viscosity is usually negligible compared with that of Gibbs elasticity. As it was shown [18] the surface viscosity affects the film behavior only in combination with surface mobility. The parameter N_{SV} does not appear in equations independently but as parameters: $N_{SV}h_s/h = \eta_s D_s/(hE_G R_c)$ and $N_{SV}b = \eta_s D/(h_a E_G R_c)$ (see [18]). Generally, the Gibbs elasticity, E_G, is very high and the latest two parameters become negligible at small N_{SV}. Therefore, the terms accounting for the surface viscosity effects can be neglected and analytical solution of the problem can be obtained. For $N_{SV} \to 0$ from Eqs. (A.5) and (A.6)(B.1)–(B.4) the dispersion relation (Eq. (18)) reduces to

$$\frac{1}{h\bar{H}_f}\frac{d\bar{H}_f}{dt} = \frac{hk^2}{12\eta}\left(\Pi' - \frac{\sigma k^2}{2}\right)[h_s + (b+1)h] - \frac{V}{h^2}\frac{h_s + 2(b+1)h}{h_s + (b+1)h} - \frac{h\Pi''}{3R_c\eta}[h_s + (b+1)h] \quad (19)$$

The right-hand side of Eq. (19) can be positive only when the first derivative of the disjoining pressure is positive and larger than the capillary term $\sigma k^2/2$. This result is in agreement with the prediction of the classical DLVO theory (see [9,16]). Also, it is important to note that the maximum of the right-hand side of Eq. (19) is achieved at wave number k_c, which is determined by the relationship

$$k_c^2 = \frac{1}{\sigma}\Pi'(h_c) \quad (20)$$

Eq. (20) represents the well-known result from the literature [9,10,16] that the critical wave number depends only on the disjoining pressure and surface tension.

If we substitute the solution Eq. (20) and the relationship for the velocity of approach, Eq. (8), calculated for $N_{SV} = 0$, into Eq. (19), the final form of the transcendental equation for the critical thickness becomes

$$\Phi_v[F - R_c\pi E(h_c)] = \frac{\pi R_c^2 h_c^3}{8\sigma}\left[(\Pi')^2 - \frac{8\sigma}{R_c}(\Pi'')\right] \quad (21)$$

where, E is the interaction energy. The mobility function, Φ_v, in the case of negligible surface viscosity effect is defined by the expression [16–18]

$$\Phi_v^{-1} = \frac{2}{\tilde{d}(b+1)}\left[\frac{\tilde{d}+1}{\tilde{d}}\ln(\tilde{d}+1) - 1\right], \quad \tilde{d} = \frac{h_s}{h(b+1)} \quad (22)$$

In the case of large interfacial elasticity the mobility parameter $\tilde{d}$ is much smaller than 1 and

$\Phi_v(\tilde{d}) \approx 1$. In the opposite case of small surfactant concentration, or when the film thickness is very small, $h_s \gg h(b+1)$ and $\Phi_v(\tilde{d}) \approx 1/(\tilde{d}\ln \tilde{d})$. Hence, the smaller the surfactant concentration the lower the dynamic pressure in the gap, and the instability occurs at higher distances.

If we specify the disjoining pressure isotherm we can calculate the critical thickness from Eqs. (21) and (22). The influence of the surfactant concentration on the critical thickness can be estimated only by numerical solution of the problem for a given isotherm and equation of state. Some analytical predictions for the influence of the van der Waals attractive disjoining pressure upon the critical thickness are possible for *tangentially immobile* interfaces. For small thickness the van der Waals interaction energy, the disjoining pressure and the corresponding derivatives can be obtained from the following relationships:

$$E = -\frac{A_H}{12\pi h^2}, \qquad \Pi = -\frac{A_H}{6\pi h^3}, \qquad \Pi' = \frac{A_H}{2\pi h^4},$$

$$\Pi'' = -\frac{2A_H}{\pi h^5} \tag{23}$$

where, A_H is the Hamaker constant. After substitution of Eq. (23) into Eq. (21) written for tangentially immobile interfaces, i.e. $\Phi_v = 1$, the particular problem for the critical thickness reduces to

$$F = \frac{R_c^2 A_H^2}{128\pi\sigma h_c^5} + \frac{5R_c A_H}{12 h_c^2} \tag{24}$$

If the driving force does not depend on the film thickness, then Eq. (24) predicts:

$$h_c^5 = \frac{R_c^2 A_H^2}{128\pi\sigma F} \quad \text{for large driving forces } F \gg F_A \tag{25a}$$

$$h_c^2 = \frac{5R_c A_H}{12F} \quad \text{for small driving forces } F \ll F_A \tag{25b}$$

where, the limiting force is derived to be $F_A \equiv 12.66(\sigma^2 R_c A_H)^{1/3}$. It is important to note that the similarity between Eq. (25b) and the analytical results for the pimple thickness, $h_{pt}^2 = A_H R_c/(12F)$ (see Eq. (19)) [18] shows that the instability appears before the pimple formation [12,18]. Next interesting conclusion is that the critical thickness is proportional to different powers of the bubble radius depending on the driving force. For example, in the case of buoyancy driven droplet approach the force is proportional to the third power of the drop radius. Therefore, for large driving forces the critical thickness depends slightly on the radius ($h_c \propto R_c^{-1/5}$), while for small driving forces it is inversely proportional to the drop radius ($h_c \propto 1/R_c$).

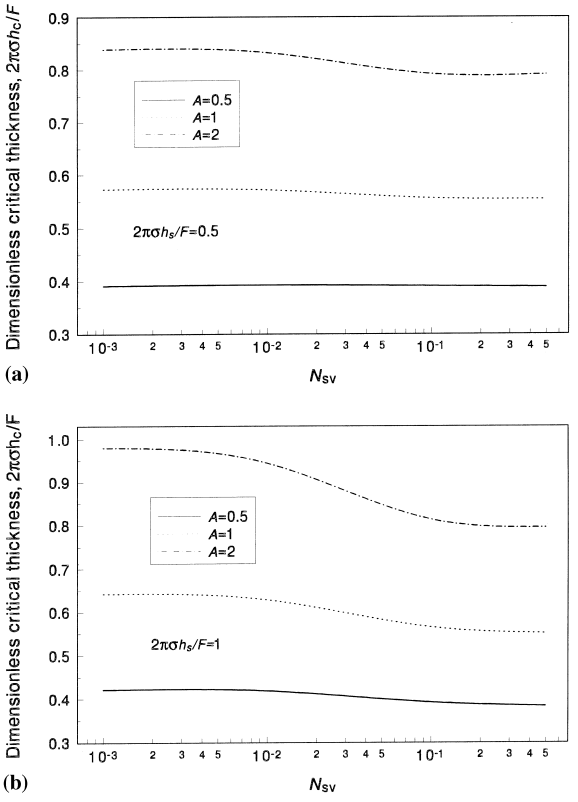

Fig. 3. Dimensionless critical thickness, $2\pi\sigma h_c/F$, as a function of the surface viscosity parameter, N_{SV}, for different values of the dimensionless Hamaker constant A, (a) the dimensionless surface diffusivity is $2\pi\sigma h_s/F = 0.5$; and (b) $2\pi\sigma h_s/F = 1$.

4. Numerical results and discussion

To show the typical influence of surfactant on the stability of the film we solved the equation (18) numerically for different dimensionless parameters. The results are presented in Fig. 3.

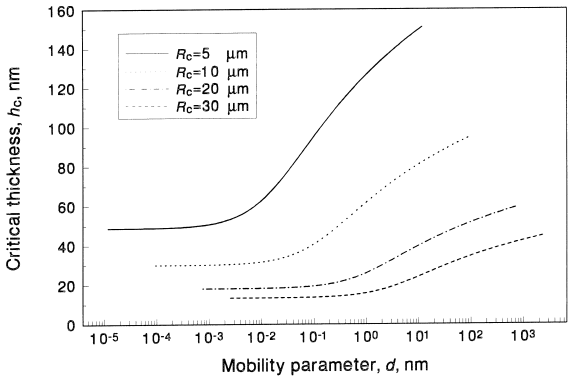

Fig. 4. Variation of the critical thickness, h_c, with the mobility length parameter, d, for $R_c = 5$, 10, 20, 30 μm.

The dependence of the dimensionless critical thickness, $2\pi\sigma h_c/F$, on the surface viscosity parameter, N_{SV}, for different values of the dimensionless Hamaker constant $A = 8R_c^2A_H(\pi\sigma)^2/F^3$ is illustrated in Fig. 3(a). The bulk and surface diffusion parameters were kept constant, $b = 0.01$ and $2\pi\sigma h_s/F = 0.5$. For calculation of the disjoining pressure only the van der Waals attraction was taken into account and the driving force, F, was assumed to be independent on the gap thickness. It is seen that with the increasing of Hamaker constant A_H (parameter A increases) the critical thickness increases. Hence, when the attractive force between the drops is higher the instabilities appear earlier. For larger attractive forces h_c decreases with increasing of the surface viscosity. It is interesting to note that in the case of high values of the Gibbs elasticity ($2\pi\sigma h_s/F = 0.5$) the critical thickness depends only slightly on the surface viscosity for the whole range of N_{SV} (see Fig. 3(a)). The suppressing effect of the Gibbs elasticity is so high that the interfaces are barely mobile and the dissipation of the energy due to the surface viscosity is small enough. On the contrary, with the increasing surface diffusivity (h_s increases), the influence of the surface viscosity becomes more considerable. In Fig. 3(b) the numerical results for the critical thickness (with surface diffusion parameter $2\pi\sigma h_s/F = 1$) are presented as a function of N_{SV}. From Fig. 3(a) and (b), for a given surface viscosity number, N_{SV}, and dimensionless parameter, A, it follows that the higher surface diffusivity leads to the higher critical thickness. When the surface diffusivity is greater the gradient of adsorption is smaller and therefore the Marangoni effect is less pronounced. This makes the interfaces more tangentially mobile, and leads to increase the influence of the surface viscosity on the critical thickness (compare with corresponding curves in Fig. 3(a) and (b) for $A = 0.5$).

The influence of the mobility length parameter, $d = h_s/(b+1)$, and the droplet radius, R_c, on the film stability for the case of negligible surface viscosity is shown in Fig. 4. The numerical solution of Eqs. (21) and (22) was made for a real system of soybean oil droplets stabilized by bovine serum albumin (BSA). To suppress the electrostatic interaction, 0.15 M sodium chloride was used (see [19,20]). The density difference, $\Delta\rho$, was measured to be 0.072 g cm^{-3}. The higher the interfacial mobility the earlier the film rupture. It is also seen that the increase of the drop radius leads to the enhancement of the stable system and the drops coalesce later (at lower critical thickness). This effect is due to the faster increase of the buoyancy force and it is analytically demonstrated in Section 3.2 for tangentially immobile interfaces.

The pimple thickness can be also interpreted as an instability of the system (see [18]), because of the very fast growth of the pimple amplitude when the van der Waals attraction is operative. Therefore, it is important to compare the the pimple thickness, h_{pt}, with the fluctuation critical thickness, h_c. The critical thickness for tangentially immobile interfaces as a function of the drop radius is plotted in Fig. 5. Therein the interfacial tension takes values $\sigma = 0.01$, 15 and 30 mN m^{-1} and all other parameters are the same as in Fig. 4. It is seen that the fluctuation critical thickness is greater than the pimple thickness in all the cases, which does not depend on the interfacial tension [18]. Therefore the instability regime starts before the pimple formation. If the drop radius changes from 40 to 100 μm the critical thickness changes slightly (see the analyti-

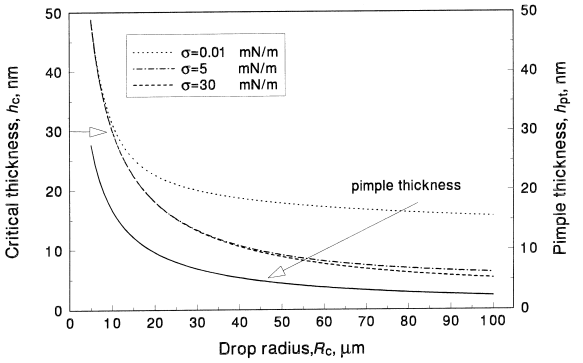

Fig. 5. Dependence of the critical thickness, h_c, on the drop radius, R_c, for different values of the interfacial tension, σ.

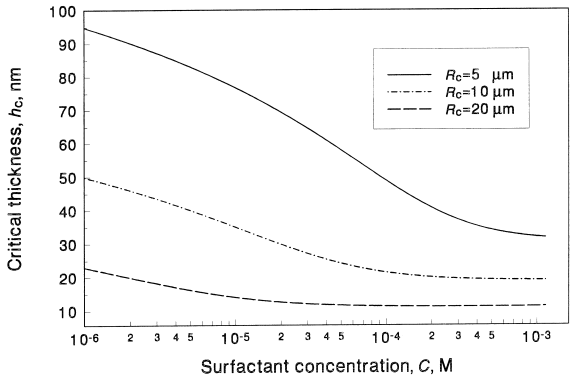

Fig. 6. Critical thickness, h_c, of decane droplets in water, stabilized by SDS + 0.1 M NaCl, as a function of the surfactant concentration, c, for $R_c = 5$, 10, 20, 30 μm.

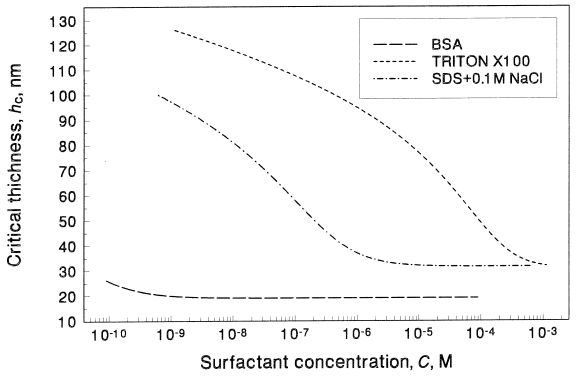

Fig. 7. Critical thickness, h_c, as a function of surfactant concentration, c, for three types of surfactants: BSA, Triton X100 and SDS + 0.1 M NaCl. The droplet radius is $R_c = 5$ μm.

cal result for tangentially immobile interfaces and large driving force in Section 3.2). The critical thickness diminishes fast for drop size from 5 to 40 μm. The interfacial tension does not influence the critical thickness significantly. Only for very low values of the interfacial tension the critical thickness increases considerably. However, $\sigma = 0.01$ mN m^{-1} is close to the spontaneous emulsification value of the interfacial tension and then other processes influence the final behavior of such systems (see [19]).

It is interesting to calculate the value of the critical thickness as a function of the surfactant concentration for typical real systems (in the presence of nonionic, ionic surfactants and protein isolates in the continuous phase). We will use the experimental data for dodecane-water interfaces in the presence of sodium dodecyl sulfate (SDS) in the bulk phase (see [21]). To suppress the electrostatic forces 0.1 M NaCl was added. The surfactant adsorption, Γ, and the interfacial tension, σ, are related with the surfactant concentration, c, by Langmuir–Szyszkowski adsorption isotherm:

$$\frac{\Gamma}{\Gamma_\infty} = \frac{c}{B+c}, \qquad \sigma = \sigma_p + k_B T \Gamma_\infty \ln\left(1 - \frac{\Gamma}{\Gamma_\infty}\right) \tag{26}$$

where, T is the temperature, k_B is the Boltzmann constant, σ_p is the interfacial tension of the pure solvent, Γ_∞ is the saturation adsorption, and B is a constant parameter, which is related with the specific energy of adsorption. The corresponding expressions for b and h_s are given in [18] (Eq. (27)). We took the following values from [19]: $\Gamma_\infty = 3.75 \times 10^{-6}$ mol m^{-2}; $B = 1.4 \times 10^{-3}$ kg m^{-3}; and $D = 6.0 \times 10^{-10}$ m^2 s^{-1}. The results for three different drop radii $R_c = 5$, 10, and 20 μm are plotted in Fig. 6. The increase of the surfactant concentration leads to a decrease of the critical thickness and the effect is more pronounced for small drops. Really, for $R_c = 5$ μm the critical thickness changes considerably in the whole range of the surfactant concentration. At bigger drop radius the increase of the critical thickness starts at lower surfactant concentration (see Fig. 6).

The dependence of the critical thickness on the surfactant concentration for different kind of surfactants is presented in Fig. 7. In our computations

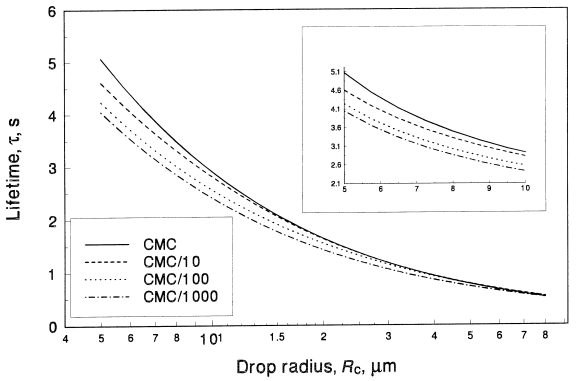

Fig. 8. Variation of the lifetime, τ, with the drop radius, R_c, for different surfactant concentrations.

we also used experimental data for the nonionic surfactant Triton X100 at the dodecane-water interface, with $\Gamma_\infty = 1.75 \times 10^{-6}$ mol m^{-2}, $B = 4.9 \times 10^{-6}$ kg m^{-3}, and $D = 2.6 \times 10^{-10}$ m^2 s^{-1} [21]. In Fig. 7 the numerical results for BSA at the air–water interface are calculated with $\Gamma_\infty = 0.38 \times 10^{-6}$ mol m^{-2}, $B = 0.124 \times 10^{-6}$ kg m^{-3}, and $D = 1.0 \times 10^{-10}$ m^2 s^{-1} [21]. The computations in all cases were for the buoyancy driving force, and for droplets with radius $R_c = 5$ μm. The influence of surfactant concentration on the critical thickness for Triton X100 becomes significant at 100 times below CMC, comparable with the corresponding behavior of the SDS. The stabilizing effect of the nonionic surfactant is more pronounced because h_c is greater. In the case of the BSA solution the critical thickness is smaller due to the greater driving force in the case of bubbles. The change of the stability is carried into effect at very low concentration. In practice such low values of surfactant concentration are not used. Therefore, it can be assumed that for proteins the critical thickness does not depend on the concentration in the region of practical importance. For protein containing systems the steric component of the disjoining pressure has to be taken into account for small gap width where the film is thermodynamically stable [22].

The experimental results [19,20,23,24] for the lifetime of oil droplets toward an oil/water interface show that the smaller the drop radius the larger the lifetime. In our numerical results (see Fig. 5) the critical thickness decreases for larger drops, i.e. the larger drops are more stable. In order to clarify this point, we calculated the life time, τ, for the hydrodynamic approach of a droplet from the given initial thickness, h_{init}, to the critical thickness, h_c:

$$\tau = \int_{h_c}^{h_{init}} \frac{dh}{V} \tag{27}$$

The numerical results for different concentrations of SDS and different radii are plotted in Fig. 8. The initial thickness for all curves was kept constant, $h_{init} = 5$ μm, and the oil phase was soybean oil. It is seen that the general trend found in the experiments from [19,20,23,24] is verified. We also observe that with the decrease of surfactant concentration the lifetime diminishes slightly. This effect is more pronounced for smaller droplets (see the inset in Fig. 8). Therefore, the mutual approach of the droplets prior to the film disrupture is the rate determining stage. The experimental results correlate with the regularities of the mutual hydrodynamic approach of droplets and there is no significant surfactant effect on the lifetime. The emulsions do not comprise single emulsion films prepared in laboratory conditions.

In order to check the differences between the transitional thickness, which we called 'critical', and the real thickness of film rupture, we performed the following calculation. We chose the critical wave number for tangentially immobile interfaces, k_c, from Eq. (20). From the dispersion relationship (Eq. (19)) we calculated the thickness, h_1, at which the relative velocity of the fluctuation growth was equal to the corresponding relative velocity of droplet approach: $-(\mathrm{d} \ln \tilde{H}_f/\mathrm{d}t)/(\mathrm{d} \ln h/\mathrm{d}t) = 1$. This means that the velocity of fluctuation growth is two times higher than the generalized Taylor velocity. They both appear in an exponential factor that is why after h_1 the fluctuations increase very fast. The ratio h_1/h_c in percents is plotted in Fig. 9 for three typical density differences, $\Delta\rho = 0.072$, 25, and 1.0 g cm^{-3}. We see that for a wide range of droplet radii from 5 to 100 μm the ratio is greater than 80%. Therefore the thickness at which the instability appears for the first time is close to the real critical one. It is easy to show that for partially mobile interfaces this difference is smaller.

5. Conclusion

A theoretical model for the calculation of the influence of surfactants on the critical distance between two colliding small bubbles is developed. It takes into account the influence of Gibbs elasticity, bulk and surface diffusion and surface viscosity. The governing dispersion equations (Eqs. (17) and (18)), derived from lubrication approximation in long wavelength approach, are used for numerical calculations to find the critical thickness. Analytical expressions, valid for tangentially immobile interfaces are derived (see Eqs. (25a) and (25b)). They can serve for simple estimation of the effect of bubbles radius and various driving forces.

The quantitative calculations (see Sections 3 and 4) show that with increasing surface mobility and the attractive disjoining pressure (e.g. van der Waals attraction) and with decreasing surface tension the critical thickness increases. In contrast, smaller driving force, larger Gibbs elasticity and surface viscosity stabilize the intervening film. All factors, which increase the hydrodynamic resistance in the gap region, lead to stabilization of the fluctuations. In the case of buoyancy driven droplet for large driving forces the critical thickness depends slightly on the radius ($h_c \propto R_c^{-1/5}$), while for small driving forces it is inversely proportional to the drop radius ($h_c \propto 1/R_c$). The pimple thickness is always smaller than the critical thickness and therefore the fluctuation instability appears before the pimple formation. The calculation shows that in the case of slightly deform bubbles the difference between the transitional and critical thickness is not so significant as for plane-parallel films [16,25] and our results can be applied for calculation of the lifetime of small bubbles and droplets.

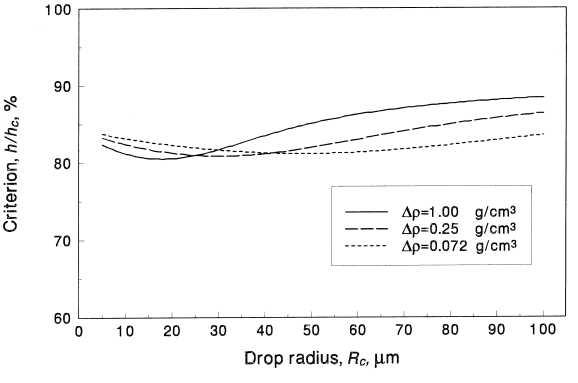

Fig. 9. The ratio h_1/h_c in percents vs. droplet radii for three typical density differences, $\Delta\rho = 0.072$, 0.25, and 1.0 g cm^{-3}.

In the case of emulsion droplets the lifetime does not influence significantly on the surfactant concentration. The regular hydrodynamic mutual approach of the droplets prior to the film disruption is the rate determining stage. The effect of surfactants (with exception for the thermodynamically stable state and strong electrostatic repulsion) on the film stability plays no substantial role in the stability of emulsions.

Acknowledgements

This study was funded by the Inco-Copernicus Project IC15CT980911. The authors are grateful for this financial support.

Appendix A. Operator equation for the dispersion relation

The definitions of operators L and M in Eqs. (15) and (16) are given by the following relationships:

$$L \equiv \frac{1}{H_{up}}\frac{\partial H_f}{\partial t} + \frac{1}{H_{up} r}\frac{\partial}{\partial r}\left[r\left(\frac{3Vr}{2H_{up}} - 2U_{up}\right)H_f\right] - \frac{1}{H_{up} r}\frac{\partial}{\partial r}\left(\frac{r H_{up}^3}{12\eta}\frac{\partial P_f}{\partial r}\right) \quad (A.1)$$

$$M \equiv \left[\frac{Vr}{2R_c H_{up}^3} + \frac{bU_{up}}{R_c(h_s + bH_{up})^2} - \frac{U_{up}}{R_c H_{up}^2}\right]H_f - \frac{H_{up}}{12\eta R_c}\frac{\partial P_f}{\partial r} \quad (A.2)$$

In order to find final equations for the fluctuations in the film profile, H_f, and the dynamic pressure, P_f, we eliminate the fluctuation of the velocity, U_f, from the integrated bulk continuity equation (Eq. (15)) and from the tangential stress boundary condition (Eq. (16)). We multiply Eq.

(15) by N_{SV}, after that we differentiate the result by r and subtract from Eq. (16). The obtained result is

$$N_{SV}\frac{\partial U_f}{\partial r}+\left[\frac{N_{SV}}{r}+\frac{H_{up}}{2r(h_s+bH_{up})}-\frac{2N_{SV}r}{R_cH_{up}}\right]U_f + \frac{R_cH_{up}}{2r}\left(N_{SV}\frac{\partial L}{\partial r}-M\right)=0 \quad (A.3)$$

In a similar way after multiplying Eq. (15) by N_{SV} and subtracting from Eq. (A.3) the final result for the velocity fluctuation, U_f, reads

$$U_f=\frac{R_c^2H_{up}^2(h_s+bH_{up})}{R_cH_{up}^2-8N_{SV}r^2(h_s+bH_{up})}\left[M - N_{SV}\left(\frac{\partial L}{\partial r}-\frac{2r}{R_cH_{up}}L\right)\right] \quad (A.4)$$

After the substitution of Eq. (A.4) into Eq. (15) the final form of Eq. (17) can be obtained.

If the Fourier–Hankel integral representations Eqs. (13) and (14) are substituted in the definitions Eqs. (A.1) and (A.2) the integral form of the operator L becomes

$$\begin{aligned}L=&\int_0^\infty\frac{1}{H_{up}}\frac{\partial\tilde{H}_f}{\partial t}J_0(kr)kdk\\&+\int_0^\infty\left\{\frac{1}{H_{up}r}\frac{\partial}{\partial r}\left[r\left(\frac{3Vr}{2H_{up}}-2U_{up}\right)\right]\right.\\&+\frac{H_{up}^2}{12\eta}k^2\left(\frac{\sigma k^2}{2}-\Pi'\right)\\&\left.+\frac{H_{up}}{3\eta R_c}\left[\left(H_{up}+\frac{3r^2}{R_c}\right)\Pi''+H_{up}\frac{r^2}{R_c}\Pi'''\right]\right\}\\&\times\tilde{H}_f\,J_0(kr)kdk\\&+\int_0^\infty\left\{\frac{3Vr}{2H_{up}^2}-\frac{2U_{up}}{H_{up}}\right.\\&\left.+\frac{rH_{up}}{6\eta R_c}\left[2H_{up}\Pi''-3\left(\frac{\sigma k^2}{2}-\Pi'\right)\right]\right\}\\&\times\tilde{H}_f\frac{\partial J_0(kr)}{\partial r}kdk\end{aligned} \quad (A.5)$$

and of the operator M it is calculated to be

$$M=\int_0^\infty\left[\frac{Vr}{2R_cH_{up}^3}+\frac{bU_{up}}{R_c(h_s+bH_{up})^2}-\frac{U_{up}}{R_cH_{up}^2}+\Pi''\frac{rH_{up}}{6\eta R_c^2}\right]\tilde{H}_f\,J_0(kr)kdk + \int_0^\infty\frac{H_{up}}{12\eta R_c}\left(\Pi'-\frac{\sigma k^2}{2}\right)\tilde{H}_f\frac{\partial J_0(kr)}{\partial r}kdk \quad (A.6)$$

The exact form Eqs. (A.5) and (A.6) give us possibility in Appendix B to calculate the limit of the image at small radial distances, i.e. at $r\to 0$.

Appendix B. Asymptotic analysis of Eq. (17) at $r\to 0$

After the long but common asymptotic analysis of Eq. (17) and taking into account the integral definitions Eqs. (A.5) and (A.6), and the solution for the unperturbed state Eqs. (6) and (7) the final form of the coefficients appearing in Eq. (18) reads

$$q_0(h)=1+8N_{SV}\left(\frac{h_s}{h}+b\right),$$
$$q_2(h)=hR_cN_{SV}\left(\frac{h_s}{h}+b\right) \quad (B.1)$$

$$\begin{aligned}g_0(h)=&\frac{V}{h}\left\{2-b-\frac{h_s}{h}+2\left(\frac{bh}{h_s+bh}+\frac{h_s}{h}+b\right)\sum_{j=0}^{\infty}ja_j\right.\\&\left.+N_{SV}\left(\frac{h_s}{h}+b\right)\left[40-32\sum_{j=0}^{\infty}ja_j\right]\right\}\\&+\frac{h^3}{3\eta R_c}\left[\Pi''\left(1+b+\frac{h_s}{h}\right)\right.\\&\left.-N_{SV}\left(\frac{h_s}{h}+b\right)(16\Pi''+8h\Pi''')\right]\end{aligned} \quad (B.2)$$

$$\begin{aligned}g_2(h)=&-\frac{h^3}{12\eta}\left(\frac{h_s}{h}+b+1\right)\Pi'\\&+N_{SV}\left(\frac{h_s}{h}+b\right)\\&\times\left[VR_c\left(5-8\sum_{j=0}^{\infty}ja_j\right)+\frac{4h^3}{3\eta}(\Pi'+h\Pi'')\right]\end{aligned} \quad (B.3)$$

$$g_4(h) = \frac{h^3\sigma}{24\eta}\left(\frac{h_s}{h} + b + 1\right) - \frac{q_2 h^2}{12\eta R_c}(8\sigma + hR_c\Pi'),$$

$$g_6(h) = \frac{\sigma h^3 q_2}{24\eta} \quad \text{(B.4)}$$

The functions (B.1)–(B.4) are used in the numerical calculations of the critical thickness in the general case (see Section 4).

References

[1] A.D. Scheludko, Adv. Colloid Interf. Sci. 1 (1967) 391.
[2] A.D. Scheludko, Proc. Konkl. Ned. Akad. Wet. 65 (1962) 87.
[3] A. de Vries, Rec. Trav. Chim. 77 (1958) 441.
[4] A. de Vries, Third Congress of Detergency Cologne, 2 (1960) 566.
[5] A. Vrij, Disc. Faraday Soc. 42 (1966) 23.
[6] A. Vrij, J. Overbeek, Am. Chem. Soc. 90 (1968) 3074.
[7] J. Lucassen, M. van den Temple, A. Vrij, F.T. Hesselink, Proc. Konkl. Ned. Acad. Wet. B73 (1970) 109.
[8] I.B. Ivanov, B. Radoev, E. Manev, A. Scheludko, Trans. Faraday Soc. 66 (1970) 1262.
[9] I.B. Ivanov, D.S. Dimitrov, Colloid Polym. Sci. 252 (1974) 982.
[10] A.K. Malhotra, D.T. Wasan, Chem. Eng. Commun. 48 (1986) 35.
[11] J.D. Chen, J.C. Slattery, AIChE J. 28 (1982) 955.
[12] S. Yiantsios, R.H. Davis, J. Colloid Interf. Sci. 144 (1991) 412.
[13] F. Leal-Calderon, T. Stora, O. Mondain-Monval, P. Poulin, J. Bibette, J. Phys. Rev. Lett. 74 (1994) 2959.
[14] O. Mondain-Monval, F. Leal-Calderon, J. Bibette, J. Phys. II France 6 (1996) 1313.
[15] K.D. Danov, D.S. Valkovska, I.B. Ivanov, J. Colloid Interf. Sci. 211 (1999) 291.
[16] I.B. Ivanov, Pure Appl. Chem. 52 (1980) 1241.
[17] I.B. Ivanov, D.S. Dimitrov, in: I.B. Ivanov (Ed.), Thin Liquid Films, Marcel Dekker, New York, 1988, p. 379.
[18] D.S Valkovska, K.D. Danov, I.B. Ivanov, Colloid Surf. A 156 (1999) 547.
[19] K.D. Danov, I.B. Ivanov, Proceedings of the 2nd World Congress on Emulsion, Bordeaux, 1997, Paper No. 2-3-154.
[20] I.B. Ivanov, K.D. Danov, P.A. Kralchevsky, Colloid Surf. A 152 (1999) 161.
[21] A. Bonfillon, D. Langevin, Langmuir 9 (1993) 2172.
[22] I.B. Ivanov, P.A. Kralchevsky, Colloid Surf. 128 (1997) 155.
[23] E. Dickinson, B.S. Murray, G. Stainsby, J. Chem. Soc. Faraday Trans. 84 (1988) 871.
[24] E.S. Basheva, T.D. Gurkov, I.B. Ivanov, G.B. Bantchev, B. Campbell, R.P. Borwankar, Langmuir 15 (1999) 6764.
[25] C. Maldarelli, R.K. Jain, in: I.B. Ivanov (Ed.), Thin Liquid Films, Marcel Dekker, New York, 1988, p. 497.